J. Biochem. **139**, 483–493 (2006)
doi:10.1093/jb/mvj062

Identification of the Substrate Interaction Region of the Chitin-Binding Domain of *Streptomyces griseus* Chitinase C

Ken-ichi Akagi[1], Jun Watanabe[2], Masashi Hara[2], Yuichiro Kezuka[3], Eriko Chikaishi[1], Tohru Yamaguchi[4], Hideo Akutsu[1], Takamasa Nonaka[3], Takeshi Watanabe[2] and Takahisa Ikegami[1,*]

[1]Laboratory of Structural Proteomics, Institute for Protein Research, Osaka University, 3-2 Yamadaoka, Suita, Osaka 565-0871; [2]Department of Applied Biological Chemistry, Faculty of Agriculture, Niigata University, 8050 Ikarashi-2, Niigata 950-2181; [3]Department of BioEngineering, Nagaoka University of Technology, Nagaoka, Niigata 940-2188; and [4]Discovery Research Laboratories, Shionogi & Co., Ltd., 12-4, Sagisu 5, Fukushima, Osaka 553-0002

Received November 4, 2005; accepted January 4, 2006

Chitinase C from *Streptomyces griseus* HUT6037 was discovered as the first bacterial chitinase in family 19 other than chitinases found in higher plants. Chitinase C comprises two domains: a chitin-binding domain ($ChBD_{ChiC}$) for attachment to chitin and a chitin-catalytic domain for digesting chitin. The structure of $ChBD_{ChiC}$ was determined by means of ^{13}C-, ^{15}N-, and ^{1}H-resonance nuclear magnetic resonance (NMR) spectroscopy. The conformation of its backbone comprised two β-sheets composed of two and three antiparallel β-strands, respectively, this being very similar to the backbone conformations of the cellulose-binding domain of endoglucanase Z from *Erwinia chrysanthemi* (CBD_{EGZ}) and the chitin-binding domain of chitinase A1 from *Bacillus circulans* WL-12 ($ChBD_{ChiA1}$). The interaction between $ChBD_{ChiC}$ and hexa-*N*-acetyl-chitohexaose was monitored through chemical shift perturbations, which showed that $ChBD_{ChiC}$ interacted with the substrate through two aromatic rings exposed to the solvent as CBD_{EGZ} interacts with cellulose through three characteristic aromatic rings. Comparison of the conformations of $ChBD_{ChiA1}$, $ChBD_{ChiC}$, and other typical chitin- and cellulose-binding domains, which have three solvent-exposed aromatic residues responsible for binding to polysaccharides, has suggested that they have adopted versatile binding site conformations depending on the substrates, with almost the same backbone conformations being retained.

Key words: cellulose, cellulose-binding domain, chitinase, chitin-binding domain.

Abbreviations: CatD, chitin-catalytic domain; CBD, cellulose-binding domain; CBM, Carbohydrate-Binding Module; ChBD, chitin-binding domain; ChiA1, Chitinase A1 from *Bacillus circulans* WL-12; ChiB, Chitinase B from *Serratia marcescens*; ChiC, Chitinase C from *Streptomyces griseus* HUT6037; EGZ, Endoglucanase Z from *Erwinia chrysanthemi*; HSQC, heteronuclear single quantum correlation; NMR, nuclear magnetic resonance; NOESY, nuclear *Overhauser* effect spectroscopy; RMSD, root mean square deviation; TOCSY, total correlation spectroscopy.

Chitin is a linear β-1,4–linked polymer of *N*-acetyl-D-glucosamine and the major constituent of the shells of crustaceans such as crabs and shrimps, the exoskeletons of insects, and the cell walls of many fungi. The quantity of chitin produced by these organisms is almost equal to that of cellulose, the second most abundant biomass on earth. Chitin differs chemically from cellulose only in that each C_2 hydroxyl (-OH) group in cellulose is replaced by an acetamide group (-$NHCOCH_3$) in chitin, and therefore the conformations of their backbones are similar to each other (*1*).

Chitinases [EC 3.2.1.14] are enzymes that catalyze the hydrolytic degradation of chitin. Chitinases exist ubiquitously, not only in organisms such as crabs, insects, fungi, and invertebrates, which contain chitin, but also in bacteria, plants, and vertebrates. Plants probably secrete chitinases to defend themselves against fungal pathogens, and bacteria produce chitinases to digest chitin, and to utilize the degradation product as carbon and energy sources. Chitinases are classified into two families, family 18 and family 19 chitinases, on the basis of the amino acid sequences of their catalytic domains according to the classification of glycosyl hydrolases by Henrissat (*2*, *3*). The catalytic domains of family 18 chitinases have $(\beta\alpha)_8$-barrel folds (*4*) exhibiting a substrate-assisted catalytic mechanism whereby the anomeric configuration of the substrate is retained (*5–7*), while the catalytic domains of family 19 chitinases have a lot of α-helices (*8*) exhibiting a general acid-and-base catalytic mechanism whereby the anomeric configuration of the substrate is inverted (*9*). The family 18 chitinases are distributed in a wide variety of organisms, while the family 19 ones were found mostly in higher plants until recently.

Chitinase C (ChiC) from a Gram-positive bacterium, *Streptomyces griseus* HUT6037, was discovered as the first chitinase that belongs to family 19 in a bacterium

*To whom correspondence should be addressed. Tel: +81-6-6879-8598, Fax: +81-6-6879-8599, E-mail: tiik@protein.osaka-u.ac.jp

other than chitinases found in higher plants (*10*). ChiC, composed of 294 amino acid residues (31.4 kDa), has two functional domains: an N-terminal chitin-binding domain ($ChBD_{ChiC}$) for attachment to chitin, and a C-terminal chitin-catalytic domain ($CatD_{ChiC}$) for breaking chitin into pieces. Since ChiC is grouped into family 19, $CatD_{ChiC}$ exhibits significant sequence similarity with the chitin-catalytic domains of other plant chitinases in family 19, and antifungal activity of ChiC has also been demonstrated (*11*). Furthermore, a transgenic rice plant that was modified to express the *chic* gene exhibited increased resistance to a fungal blast disease (*12*).

The N-terminal $ChBD_{ChiC}$ comprises 52 amino acid residues, *i.e.*, from Ala30 to Gly81, with a molecular weight of 5,981. In spite of the high sequence similarity between $CatD_{ChiC}$ and the chitin-catalytic domains of other plant chitinases in family 19, the sequences of their chitin-binding domains are significantly different. ChBDs of plant chitinases belong to CBM family 18 (http://afmb.cnrs-mrs.fr/CAZY/) (*13*), among which class I and IV plant enzymes (*14*) are rich in cysteine residues and are referred to as the hevein domain or the wheat germ agglutinin domain (*15*). By contrast, $ChBD_{ChiC}$ belongs to CBM family 5, exhibiting a sequence similarity to those found in some bacterial family 18 chitinases, cellulases, and proteases (Fig. 1). For example, the sequence alignment of $ChBD_{ChiC}$ with ChBD of chitinase A1 from *Bacillus circulans* WL-12 ($ChBD_{ChiA1}$) (*16*, *17*) and the cellulose-binding domain of endoglucanase Z from *Erwinia chrysanthemi* (CBD_{EGZ} or Cel5) (*18*), respectively, showed similarities of 24 and 21 %. Although $ChBD_{ChiC}$ is not of a plant type, $ChBD_{ChiC}$ still helps $CatD_{ChiC}$ catalyze the digestion of chitin by hitching the substrate, as demonstrated using ChiC that lacked $ChBD_{ChiC}$, which exhibited decreased antifungal activity, *i.e.*, less than one-tenth (*19*).

Kezuka *et al*. recently determined the crystal structure of ChiC [*Acta Cryst.* (2005) **A61**, C192 for XX Congress of the IUCr2005], and we herein report the solution structure of its chitin-binding domain determined by

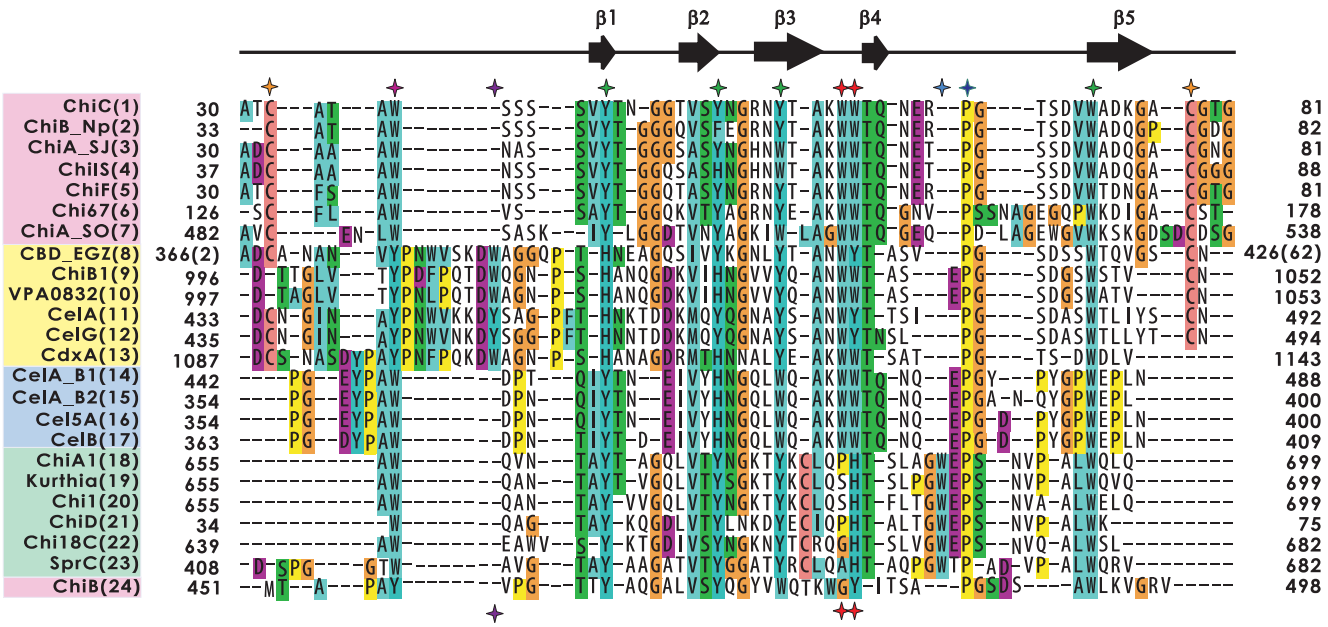

Fig. 1. **Alignment of the amino acid sequences of various chitin- and cellulose-binding domains.** The sequences of ChBDs and CBDs, which belong to CBM family 5 or 12, were at first aligned using ClustalW (ver. 1.83) (*45*), and then further modified based on the alignment of the known three-dimensional structures of $ChBD_{ChiC}$ (#1 in this figure, PDB accession code: 2D49), $ChBD_{ChiA1}$ (#18, 1ED7), $ChBD_{ChiB}$ (#24, 1E15), and CBD_{EGZ} (#8, 1AIW) using the Dali server (ver. 2.0) (*46*). Amino acid residues that have been well conserved among the species in the evolutionary process are indicated by colored backgrounds. The listed ChBDs and CBDs can be classified on the basis of their sequences and conformations (see text), and their protein names are grouped with different colors. The important residues for the classification are indicated by the stars at the top, corresponding to the residues shown in Fig. 5b. The positions of the three aromatic residues that are exposed to the solvent and involved in binding to a substrate, as observed in most cellulose-binding domains, are indicated by the stars at the bottom. The N-terminal beginning and C-terminal ending residue numbers of each domain are shown on the left and right, respectively. The secondary structures at the top are for $ChBD_{ChiC}$. The sequences listed are those of *Streptomyces griseus* HUT6037 chitinase C (ChiC, 1), *Nocardiopsis prasina* family19 chitinase (ChiB_Np, 2), *Streptomyces* sp. J-13-3 chitinase precursor (ChiA_SJ, 3), *Streptomyces* sp. MG3 chitinase IS (ChiIS, 4), *Streptomyces griseobrunneus* chitinase (ChiF, 5), *Doohwaniella chitinasigens* chitinase Chi67 (Chi67, 6), *Shewanella oneidensis* chitinase A (ChiA_SO, 7), *Erwinia chrysanthemi* endoglucanase Z precursor (CBD_EGZ, 8), *Vibrio harveyi* chitinase B (ChiB1, 9), *Vibrio parahaemolyticus* chitodextrinase (VPA0832, 10), *Pseudoalteromonas* sp. MB-1 cellulase (CelA, 11), *Alteromonas haloplanktis* cellulase precursor (CelG, 12), *Saccharophagus degradans* 2–40 chitodextrinase (CdxA, 13), *Bacillus* sp. (strain N-4/JCM9156) endoglucanase A (CelA_B1, 14), *Bacillus* sp. (strain N-4/JCM9156) endoglucanase A (CelA_B2, 15), *Bacillus agaradhaerens endoglucanase 5A (Cel5A*, 16), *Bacillus* sp. (strain N-4/JCM9156) endoglucanase B (CelB, 17), *Bacillus circulans* chitinase A1 precursor (ChiA1, 18), *Kurthia zopfii* chitinase (Kurthia, 19), *Bacillus circulans* chitinase (Chi1, 20), *Bacillus circulans* chitinase D precursor (ChiD, 21), *Clostridium paraputrificum* chitinase 18C (Chi18C, 22), *Streptomyces griseus* serine protease (SprC, 23), and *Serratia marcescens* chitinase B precursor (ChiB, 24).

NMR. Surprisingly, both structures revealed that $ChBD_{ChiC}$ has only two aromatic residues that are exposed to the solvent unlike CBD_{EGZ}, which has three such residues. These residues on CBD_{EGZ} were known to interact directly with cellulose, but it was unknown whether or not the two aromatic residues on $ChBD_{ChiC}$ were also actually involved in the interaction with the substrate, chitin. To clarify this point, we performed NMR spectroscopy, and observed a direct interaction between $ChBD_{ChiC}$ and a soluble form of chitin. Fortunately, $ChBD_{ChiC}$ binds not only to insoluble solid-state chitin but also to soluble forms of chitin including an oligosaccharide. Solution-state NMR spectroscopy is a powerful tool for determining the interaction surfaces on proteins with soluble forms of substrates. In addition, we analyzed the dynamics through ^{15}N-spin relaxation to discuss the possibility of any conformational change such as an induced-fit phenomenon occurring upon interaction with chitin.

EXPERIMENTAL PROCEDURES

Sample Preparation—Cells of *Escherichia coli* strain BL21(DE3) transformed with the expression pET22b(+) plasmid (Novagen) containing the gene of $ChBD_{ChiC}$ were grown in an M9 minimal medium containing 0.5 g/liter $^{15}NH_4Cl$ and 1.0 g/liter [*U*-$^{13}C_6$]D-glucose as sole nitrogen and carbon sources, respectively, to obtain doubly ^{15}N- and ^{13}C-labeled proteins. For the expression of uniformly ^{15}N-labeled proteins, $^{13}C_6$-labeled D-glucose was replaced with 4.0 g/liter D-glucose and 0.1% glycerol was added to the minimal medium. The cells were incubated at 37°C with shaking. The expression of the proteins was induced by the addition of isopropyl-D-thiogalactopyranoside (IPTG) to a final concentration of 1.0 mM when the cell density reached an absorbance value of 0.5 at 600 nm, and the bacteria were grown for an additional three hours at 37°C. The sequence of the expressed protein comprised Ala30 to Gly81 of ChiC, with additional methionine and serine residues attached to the N- and C-termini, respectively. The cells were collected by centrifugation, and disrupted by sonication in a 100 mM Tris-HCl buffer (pH 8.0) comprising 400 mM KCl, 10 μM 4-(2-aminoethyl)-benzene sulfonyl fluoride hydrochloride (AEBSF), and 1 mM EDTA. The crude substances were salted out from the sonicated solution with 80% saturated ammonium sulfate. The precipitate was suspended in 200 ml (per liter culture medium) of a 1 mM potassium-phosphate (K_2HPO_4-KH_2PO_4) buffer (pH 6.0). $ChBD_{ChiC}$ was purified mainly by utilizing its affinity to solid chitin; it binds to chitin around pH 6 and unbinds around pH 3. The solution was loaded onto a chitin (Funakoshi, KIM K-02) open-column equilibrated previously with a 20 mM phosphate buffer (pH 6.0). The column was washed with the same buffer containing 1 M KCl and then with a 20 mM sodium-acetate buffer (pH 5.5). $ChBD_{ChiC}$ was eluted with 20 mM acetic acid (pH 3.0). The elute was dialyzed against a 1 mM phosphate buffer (pH 6.0), and then passed through a hydroxyapatite column (Seikagaku, 800200) with a 1 mM phosphate buffer (pH 6.0) to remove residual impurities. The fractions containing $ChBD_{ChiC}$ were collected and the proteins were concentrated with a Centricon-YM3 (Amicon. molecular cutoff, 3,000) to about 1 mM. The solvent was simultaneously exchanged with a 20 mM potassium phosphate buffer (pH 6.0) containing 1 mM DTT, 0.02% (w/w) NaN_3, and 10% D_2O for the NMR experiments. Protein concentrations were estimated using the calculated molar absorption coefficient at 280 nm (A_{280}) of 26,720.

Resonance Assignments—NMR spectra were acquired at 303 K with Bruker DRX-600, DRX-500, and AV-400M spectrometers. For assignment of the ^{1}H, ^{15}N, and ^{13}C resonances, a series of two- (2D) and three-dimensional (3D) experiments were performed: 2D ^{15}N-^{1}H-heteronuclear single quantum correlation (HSQC), ^{13}C-^{1}H-HSQC, ^{1}H-^{1}H-total correlation spectroscopy (TOCSY), 3D ^{15}N-edited nuclear *Overhauser* effect spectroscopy (NOESY) with a mixing time of 100 ms, ^{15}N-edited TOCSY with a mixing time of 72.1 ms, HNCO, HN(CA)CO, CBCA(CO)NH, CBCANH, HBHA(CBCACO)NH, HCCH-TOCSY, C(CO)NH, and H(CCO)NH with a mixing time of 20.2 ms.To determine the correlation between ^{1}H and ^{13}C spins that were directly bound to each other in side-chains, a 4D HCCONH spectrum was also acquired. Most of the NMR experiments involved the sensitivity-enhancement and gradient-echo methods for the indirect ^{15}N dimensions. (*21*). The chemical shifts of the ^{1}Hδ/ϵ spins in the aromatic residues were assigned by means of 2D (Hβ)Cβ(CγCδ)Hδ and (Hβ)Cβ(CγCδCϵ)Hϵ experiments (*22*). The NMR data were processed and analyzed using the NMRPipe (*23*) and Sparky (*24*) software packages, respectively. For extraction of the coupling constants of $3J_{NC\gamma}$ and $^3J_{CoC\gamma}$ of aromatic side-chains, 2D HN(Cγ) and HN(COCγ) spectra were acquired (*25*). For each amide resonance, peak heights were measured, and the ratio between the intensity for the coupling-active spectrum and that for the reference spectrum was calculated for each experiment. Comparison between the measured ratios and those calculated with trial *J* coupling constants allowed the estimation of experimental $^3J_{NC\gamma}$ and $^3J_{CoC\gamma}$ coupling constants. The combination of the two constants allowed the selection of one of the χ_1 angles among the –60°, 60°, and 180° rotameric states for each aromatic residue.

Structure Calculation—The nuclear *Overhauser* effect (NOE) connectivities derived from strong, medium, and weak cross peaks were categorized and assumed to correspond to the upper limits for the interproton distance restraints of 3.0, 4.0, and 5.0 Å, respectively. Pseudo-atom corrections were applied to the upper bound restraints involving methyl, methylene, and aromatic ring protons as described (*26*). The distance restraints for the hydrogen-bonds were applied for slowly exchanging amides, *i.e.*, 2.8–3.3 Å for N-O pairs and 1.8–2.3 Å for H-O pairs, after the root mean square deviation (RMSD) value for the overlaid backbone atoms of calculated structures reached 1.0 Å. The acceptors of the hydrogen-bonds in β-sheets were determined on the basis of the characteristic backbone torsion angles, and short and medium range NOE patterns (Fig. 2a). The restraint for the disulfide bond was included after the backbone RMSD reached 1.0 Å according to the CYANA (*27*) standard procedure, where three restraints were applied between residue numbers *i* and *j* in the form of $2.0 \leqslant d(S_{i\gamma}, S_{j\gamma}) \leqslant 2.1$ Å, $3.0 \leqslant d(C_{i\beta}, S_{j\gamma}) \leqslant 3.1$ Å, and $3.0 \leqslant d(S_{i\gamma}, C_{j\beta}) \leqslant 3.1$ Å. The methyl pairs of all three valine residues were assigned stereospecifically using 15% fractionally

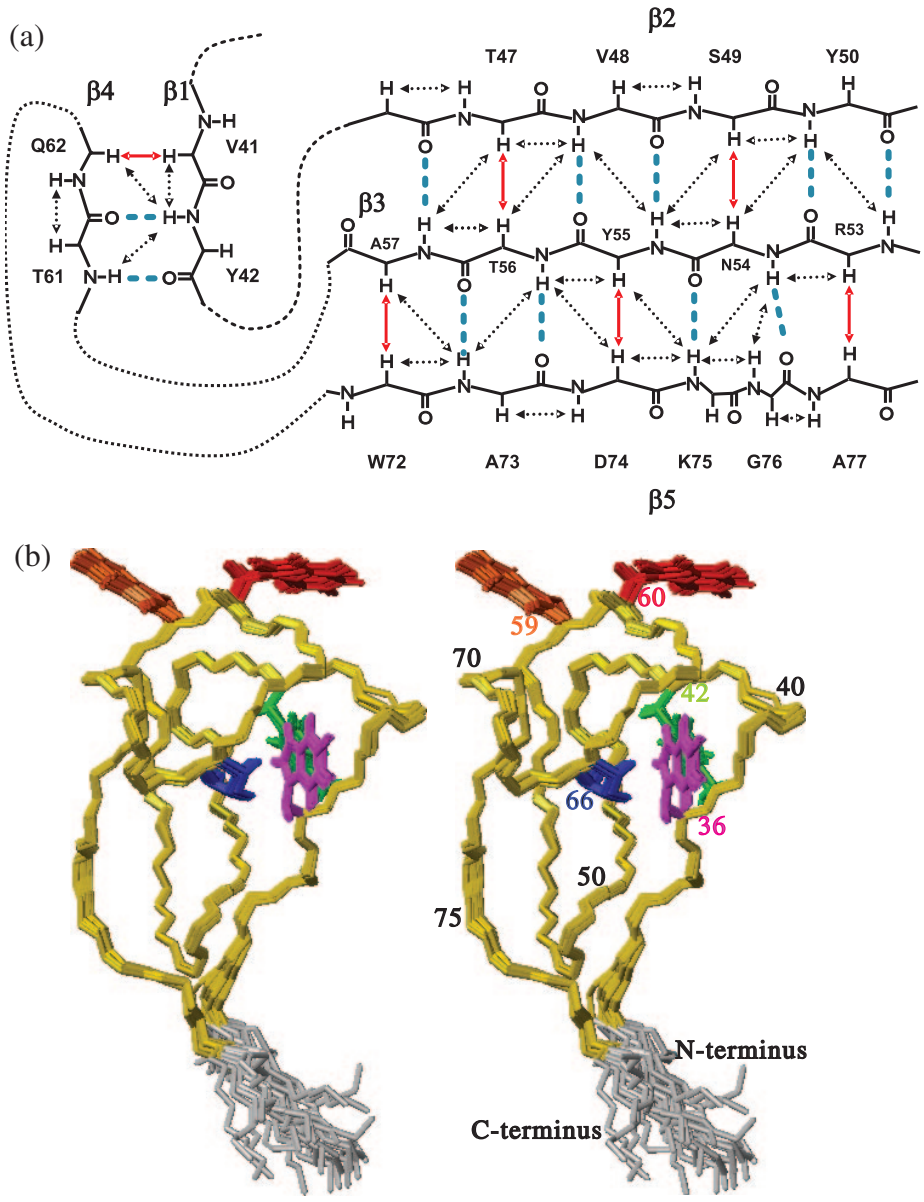

Fig. 2. **Solution structure of $ChBD_{ChiC}$.** (a) The distance information defining the β-sheets. The intra and interstrand NOEs are indicated by dashed arrows. The interstrand NOEs observed between Hα nuclei, which are typical of β-sheets, are indicated by red arrows. The hydrogen-bonds used for the structure calculations are indicated by cyan dotted lines. (b) The best-fit superposition of the final 30 structures, which were calculated with CYANA-2.1, is shown in stereo-view. The backbone heavy atoms in the region from Thr31 to Gly79 are superimposed. The colored residues are Trp36 (purple), Tyr42 (green), Trp59 (orange), Trp60 (red), and Pro66 (blue). The figures were produced using MOLMOL (*47*).

^{13}C-labeled $ChBD_{ChiC}$ (*28*). The backbone torsion angles were predicted using TALOS software (*29*) with the assigned chemical shifts of ^{13}Cα, ^{13}Cβ, ^{13}Co, ^{1}Hα, and ^{15}N, which were calibrated with 2,2-dimethyl-2-silapentane-5-sulfonate sodium salt (DSS). The restraints for the backbone dihedral angles, ϕ and ψ, were applied in the form of the average ± once or twice the standard deviation as long as TALOS categorized the corresponding angles as "Good" or "New," respectively. The structures were calculated by means of molecular dynamics in a torsion angle space with 25,000 steps using CYANA-2.1 software. After well-converged structures with an RMSD of < 1.0 Å for the backbone atoms had been obtained, the pseudo-atom corrections for the center averaging were removed and, instead, the r^{-6} sum averaging method for the degenerate protons in the methyl and aromatic protons, and the floating chirality approach for the diastereotopic groups such as methylene protons were applied as the default in the CYANA calculations. The 30 structures with the lowest target functions among the 100 calculated were further analyzed. The secondary structures were determined on the basis of the backbone hydrogen-bond patterns, NOE connectivities, and the results of AQUA-PROCHECK-NMR analysis (*30*).

Titration with an Oligosaccharide—A stock solution of 7 mM chitohexaose, which comprised six *N*-acetyl-D-glucosamines linked by β-1,4 glycosidic linkages, was added repeatedly to 0.7 mM ^{15}N-labeled $ChBD_{ChiC}$, and then a series of 18 ^{1}H-^{15}N HSQC spectra were obtained with a DRX-600 spectrometer at 303 K until the stoichiometry of chitohexaose over $ChBD_{ChiC}$ reached 6.5. Similarly, 0.5 mM ^{15}N- and ^{13}C-labeled $ChBD_{ChiC}$ was titrated with a stock solution of 5 mM chitohexaose, and then ^{1}H-^{13}C-HSQC spectra were obtained until the stoichiometry of chitohexaose over $ChBD_{ChiC}$ reached 9.0. The chemical shifts of the backbone and side-chain ^{1}H-^{15}N and ^{1}H-^{13}C spins were assigned by tracing the corresponding peaks in the ^{1}H-^{15}N- and ^{1}H-^{13}C-HSQC spectra,

respectively, measured at various concentrations of chitohexaose. All chemical shift changes were fitted through a non-linear least square fitting procedure with Mathematica software to the function of the form,

$$\delta = \delta_{OBS}-\delta_E = \frac{\delta_{SAT}}{[ChiC_t]}\cdot\left\{\frac{K_d + [ChiC_t] + [Hex_t]}{2}\cdot - \frac{\sqrt{(K_d + [ChiC_t] + [Hex_t])^2-4\cdot[ChiC_t]\cdot[Hex_t]}}{2}\right\}$$

where δ_{OBS} represents the chemical shifts observed for $ChBD_{ChiC}$ at the total concentrations of $ChBD_{ChiC}$ and chitohexaose at $[ChiC_t]$ and $[Hex_t]$, respectively, and δ_E and δ_{SAT} represent those in the absence of chitohexaose and in the presence of an infinite amount of chitohexaose, respectively.

Relaxation Analyses—Spectra for ^{15}N longitudinal relaxation times, T_1, ^{15}N transverse relaxation times, T_2, and $\{^1H\}$–^{15}N steady-state heteronuclear NOE values were acquired at 303 K, using 2.0 mM ^{15}N-labeled $ChBD_{ChiC}$ and a Bruker DRX-500 NMR spectrometer. The pulse sequences included the combination of sensitivity-enhancement and gradient-echo for the indirect ^{15}N dimensions (*31*). T_1 was deduced from the data with 15 relaxation delays, *i.e.*, 5, 25, 45, 65, 145, 185, 245, 365, 525, 755, 1145, 1255, 1500, 1655, and 1905 ms, and T_2 from the data with 20 relaxation delays, *i.e.*, 7.5, 22.5, 37.5, 52.5, 67.5, 82.5, 97.5, 112.5, 142.5, 172.5, 202.5, 232.5, 262.5, 307.5, 337.5, 382.5, 412.5, 457.5, 532.5, and 607.5 ms. In the heteronuclear NOE experiment, ^1H saturation for 5.0 s during the relaxation delay was applied for NOE enhancement. The other parameters for these measurements were set as described previously (*31*). The peak height at a fixed amide resonance position for each residue was collected from a series of spectra. Each T_1 or T_2 value was determined by fitting a series of measured intensities to a two-parameter function in the form of $I(t) = I_0 \exp(-t/T_{1,2})$, where $I(t)$ is the intensity after time delay t, and I_0 the intensity at time zero. The uncertainties of the T_1 and T_2 values were estimated by means of Monte-Carlo simulations. The $\{^1H\}$-^{15}N steady-state NOE values were determined from the ratios of the peak intensities with and without proton saturation ($I_{NOE}/I_{NON\text{-}NOE}$). The overall rotational correlation time, τ_m, was obtained from the mean of the T_1/T_2 ratios that were limited to within one standard deviation (*31*). The model-free analysis developed by Lipari and Szabo (*32*), with the isotropic rotational diffusion model assumed, was performed with the Tensor2 program (*33*).

RESULTS

Sample Preparation—From a culture in 1 liter M9 minimum medium, 0.78 mg of doubly ^{15}N- and ^{13}C-labeled protein and 7.5 mg of singly ^{15}N-labeled protein were obtained. The yield of the expressed $ChBD_{ChiC}$ protein was very dependent on the amount of carbon present in the medium. A high level of purity was confirmed by the single band corresponding to the molecular weight of $ChBD_{ChiC}$ observed on sodium dodecyl sulfate–polyacrylamide gel electrophoresis (SDS-PAGE).

Resonance Assignments—Almost all the backbone resonances were assigned sequentially by means of the combination of 3D spectra obtained using ^{15}N- or ^{15}N-,^{13}C-labeled $ChBD_{ChiC}$. Excluding the N-terminal methionine, all the observable peaks derived from the ^1H-^{15}N, $^{13}C\alpha$, $^{13}C\beta$, ^{13}Co, and ^1H-^{13}C nuclei in the backbone and aliphatic side-chains were assigned. We observed peaks derived from the $^{13}C\alpha$ and $^{13}C\beta$ nuclei of the N-terminal methionine residue, whose resonances were correlated with those of the amide group of the second alanine in the 3D CBCA(CO)NH spectrum. The fact that the intensities of these peaks were comparable to those of the $^{13}C\alpha$ and $^{13}C\beta$ peaks of the other residues suggested that the first methionine was preserved in $ChBD_{ChiC}$ expressed in *E. coli* cells. The assignment of the aromatic ^1H-^{13}C nuclei accounted for 50%. The results of the assignments of the ^1H-^{15}N spins are shown on a 2D ^1H-^{15}N HSQC spectrum of $ChBD_{ChiC}$ in Fig. 3a.

Structure Determination—The structures of $ChBD_{ChiC}$ were calculated by CYANA, using NOE-derived 574 distance restraints obtained in the 3D ^{15}N-edited NOESY, 3D ^{13}C-edited NOESY, and 2D ^1H-^1H NOESY experiments, 44 ϕ and 43 ψ dihedral angle restraints predicted on the basis of the backbone (^{15}N, $^{13}C\alpha$, $^{13}C\beta$, 13Co, and $^1H\alpha$) chemical shift deviations from those of random coils using TALOS (*29*), 5 χ_1 angle restraints for aromatic residues, 15 hydrogen-bond restraints for residues that exhibited slow proton/deuteron exchange rates in the amide hydrogens, and one disulfide bond restraint between Cys32 and Cys78 determined by their characteristic Cα and Cβ chemical shifts (*34*) (Table 1). After calculation of 100 structures, the 30 of them with the lowest target functions were extracted, which did not exhibit a distance restraint violation of >0.1 Å, or a dihedral angle restraint violation of >2.0°. No ϕ or ψ angle was found in the disallowed region of the Ramachandran plot. The RMSD for the backbone atoms and all the heavy atoms from Thr31 to Gly79 were 0.19 and 0.68 Å, respectively (Fig. 2b).

$ChBD_{ChiC}$ had a compact and globular conformation, comprising two β-sheets, as shown in Fig. 2. One of them was composed of three antiparallel β-strands designated as β2 (Thr47–Tyr50), β3 (Arg53–Ala57), and β5 (Trp72–Ala77), and the other was composed of two antiparallel β-strands designated as β1 (Val41–Tyr42) and β4 (Thr61–Gln62). Fig 2a shows the observed hydrogen-bond networks and NOE connectivities, especially between Hα spins in the neighboring strands, which were very characteristic of β-sheet regions. We judged that a β-sheet was formed between β1 and β4 in light of the slow amide-hydrogen exchange rates of Tyr42 in β1 and Thr61 in β4, and of an NOE observed between the Hα nuclei of Val41 in β1 and Gln62 in β4. However, the intensity of this NOE peak was actually weaker than those of the others, and thus the distance between these Hα nuclei was greater (3.02 Å) than the average distance in a normal antiparallel β-sheet (2.3 Å), or the two strands may be fluctuating in solution. Because of this slight deviation from the normal β-sheet conformation, program Chimera (*35*) did not recognize a β-sheet in this region, as shown in Fig. 5a. In the chitin-binding domain of chitinase B from *Serratia marcescens* ($ChBD_{ChiB}$) (*36*), the corresponding region does not form a β-sheet. Consequently, whether or not a

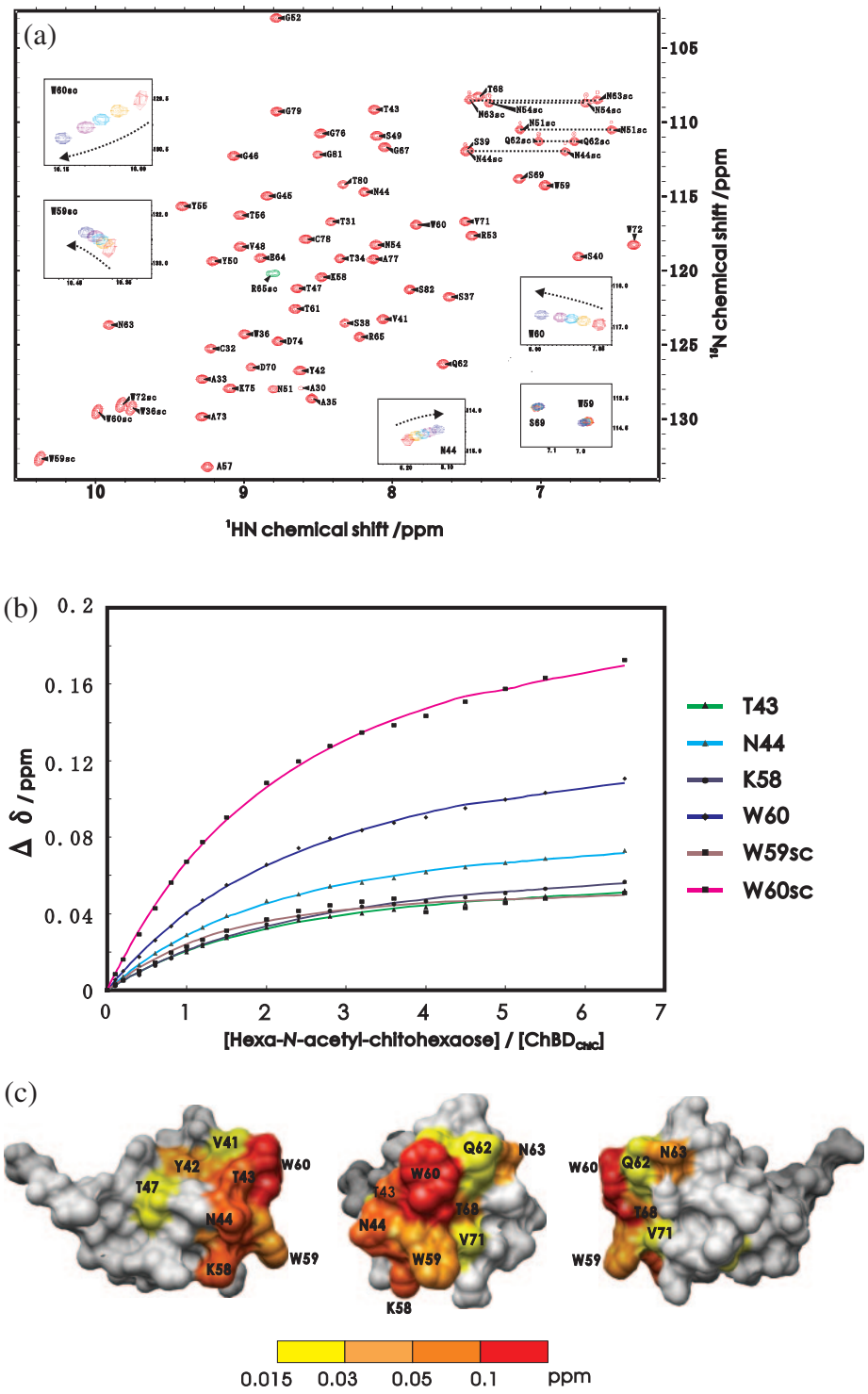

Fig. 3. **Perturbation of chemical shifts of ChBD$_{ChiC}$ upon interaction with hexa-*N*-acetyl-chitohexaose.** (a) A 2D ^{1}H-^{15}N HSQC spectrum of ^{15}N-labeled ChBD$_{ChiC}$, obtained at 303 K with a Bruker DRX-500 spectrometer, is shown with the assignment of each peak to the corresponding amide group indicated by single-letter codes and residue numbers. The assignments of the ^{1}H and ^{15}N nuclei in the side-chains of asparagines, glutamines, and tryptophans are additionally labeled "sc." The green peak was folded from the higher field in the ^{15}N dimension, resonating originally at 86.2 ppm. From its characteristic ^{15}N chemical shift and the results of analysis of the 3D-NOESY-^{15}N-HSQC spectrum, it was expected to be assigned to the imino group of Arg65. The insets are overlaid magnified spectra that were obtained with various molar ratios of chitohexaose to ChBD$_{ChiC}$ (red: 0, orange: 0.6, green: 1.2, violet: 2.0, and blue: 6.5), showing the chemical shift changes of ChBD$_{ChiC}$ in the directions indicated by the dashed arrows as the amount of chitohexaose in the solution increased. (b) Titration curves of chemical shift changes observed for several residues of ^{15}N-labeled ChBD$_{ChiC}$. The chemical shift changes of the indicated residues are plotted as a function of the molar ratios of hexa-*N*-acetyl-chitohexaose to ChBD$_{ChiC}$. Weighted averages of ^{1}H and ^{15}N chemical shift changes, Δδ(ppm), were calculated with the function $[(\delta^{1}H)^2/2 + (\delta^{15}N/5)^2 /2]^{1/2}$. The solid curves represent the equation for the titration that fit the data best. (c) Mapping of the perturbed residues on the solution structure of ChBD$_{ChiC}$.

β-sheet exists between β1 and β4 in ChBD$_{ChiC}$ could depend on the conformational definition of β-sheets.

TITRATION WITH CHITOHEXAOSE

To determine which part of ChBD$_{ChiC}$ actually interacts with chitin, soluble hexa-*N*-acetyl-chitohexaose was added to a solution containing ^{15}N-labeled ChBD$_{ChiC}$, and then a series of 2D ^{1}H-^{15}N-HSQC spectra of ChBD$_{ChiC}$ were acquired with various molar ratios of chitohexaose to ChBD$_{ChiC}$. We observed that as the stoichiometry of chitohexaose in the solution increased, some signals of ChBD$_{ChiC}$ moved to a larger extent (Fig. 3, a and b), and therefore we judged that the interaction between chitohexaose and ChBD$_{ChiC}$ was in a fast exchange mode with respect to the chemical shift time scale. Although

Table 1. **Statistics for the final 30 structures of $ChBD_{ChiC}$.**

Distance restraints	
Intraresidue ($i-j=0$)	220
Sequential ($\|i-j\|=1$)	147
Medium range ($\|i-j\|<5$)	34
Long range ($\|i-j\|>4$)	173
Hydrogen-bonds	15
Disulfide bond	1
Total	590
Dihedral angle restraints	
ϕ	44
ψ	43
χ_1	5
Total	92
Mean r.m.s. deviations from the experimental restraints	
Distance (Å)	0.0074 ± 0.0004
Dihedral angle (°)	0.3002 ± 0.0343
Ramachandran plot	
Residues Ala30–Gly81	
% residues in	
most favorable regions	71.2
additionally allowed regions	28.8
generally allowed regions	0
disallowed regions	0
Atomic r.m.s. differences (Å)	
Residues Thr31–Gly79	
R.m.s. deviations from the mean coordinates	
Backbone heavy atoms (N, Cα, and Co)	0.19 ± 0.05
Heavy atoms	0.68 ± 0.08

saturation could not be reached even with the highest molar ratio in this experiment, the equation representing the titration curve fitted well to the experimental data, providing a dissociation constant (K_d) of 1.57 mM ± 0.25 (one standard deviation) from the statistics of 11 titration curves (Fig. 3b). Itoh *et al*. (*19*) have also investigated the interaction between $ChBD_{ChiC}$ and chitohexaose by means of an isothermal titration calorimetry (ITC) assay. Unlike in the case of $ChBD_{ChiA1}$ from *Bacillus circulans* WL-12 (*20*), which does not interact with soluble chitooligomers, they detected a significant amount of heat generated upon the interaction between $ChBD_{ChiC}$ and chitohexaose. This ITC experiment determined the dissociation constant (K_d) to be 2 mM, which was very consistent with the K_d value (1.57 mM) determined in our NMR titration experiment.

Figure 3c visualizes the mapping of the residues that underwent significant perturbations in their chemical shifts on the tertiary structure of $ChBD_{ChiC}$. These residues were distributed in a patch containing the two aromatic residues exposed to the solvent (Trp59 and Trp60). Trp60 was influenced most, and other residues including Thr43, Asn44, Lys58, and Thr68, which were located around the two aromatic residues, were moderately influenced. We performed a similar experiment using a series of 2D ^{1}H-^{13}C HSQC spectra, where chemical shift perturbations in the side-chains of Val41, Thr43, Val71, and Lys58 were observed. These residues also exhibited perturbations in the chemical shifts of their amide groups. We observed chemical shift changes in some ^{1}H-^{13}C nuclei that were supposed to belong to the aromatic rings of Trp59 and Trp60, but we could not assign them unambiguously due to severe overlapping of their resonances. The overall results clearly show that Trp59 and Trp60 directly interact with chitin, and that the surrounding residues may also be involved in the interaction with the substrate through hydrogen-bonding.

In addition to using chitohexaose, we performed similar chemical shift perturbation experiments using chitotriose (tri-*N*-acetyl-D-chitotriose) and chitotetraose (tetra-*N*-acetyl-D-chitotetraose). Chitotriose or chitotetraose was added to the solution of $ChBD_{ChiC}$ such that the protein concentration was 0.6 mM, and the stoichiometry of each chitooligomer over $ChBD_{ChiC}$ was 14 and 10, respectively. The largest resonance perturbations were observed for the main-chain and side-chain amide groups of Trp60, *i.e.*, 0.0090 (-NH in the main-chain) and 0.0094 ($-NH_{\epsilon}{}^{1}$ in the side-chain) ppm for chitotriose, and 0.0439 (main-chain) and 0.0581 (side-chain) ppm for chitotetraose. The degrees of these perturbations corresponded to 6%, for chitotriose, and 33%, for chitotetraose, of those estimated assuming that the same stoichiometry of chitohexaose was added. These results indicated that the affinity of chitooligomers to $ChBD_{ChiC}$ depended on their lengths, shorter ones exhibiting lower affinity. Although much higher affinity was expected for chitooligomers longer than chitohexaose, the low solubility of such substrates prohibited further research.

The affinity of $ChBD_{ChiC}$ to solid chitin has been confirmed to be much higher than that to chitohexaose through a competitive binding assay by Itoh *et al*. (*19*), which demonstrated that chitohexaose prevented $ChBD_{ChiC}$ from binding to solid chitin (powdered prawn-shell chitin) only by 5%. They also observed that the interaction of $ChBD_{ChiC}$ with chitin depended on the degree of acetylation of the substrates by comparing the affinities to chitins with various degrees of deacetylation.

BACKBONE DYNAMICS

Figure 4 shows the experimentally obtained relaxation times, T_1 and T_2, and NOE values for the amide ^{15}N spins of 52 residues, the exceptions being the first methionine and Pro66. The rotational correlation time of $ChBD_{ChiC}$ was estimated to be 2.33 ns. Generally, small NOEs, long T_2 times, and small squared order parameters (S^2) reflect the presence of picosecond (ps) to nanosecond (ns) time scale motion. Such phenomena were observed for the N-terminal one or two, and C-terminal three residues, suggesting that both terminal regions are more flexible in terms of the fluctuations on ps to ns time scales than the other parts. It should be noted that the T_1 times for these terminal regions were longer than the others because the correlation time of $ChBD_{ChiC}$ is relatively short; for macromolecules containing, for example, more than 100 residues, the opposite tendency would be observed for the T_1 times.

As shown in Fig. 4, S^2 values as high as about 0.8 were observed throughout the sequence except for the above mentioned terminal regions. Furthermore, for the R_{ex} term, which represents the scale of conformational or chemical exchange in a time range of microsecond (μs) to millisecond (ms), no significant value was detected with the

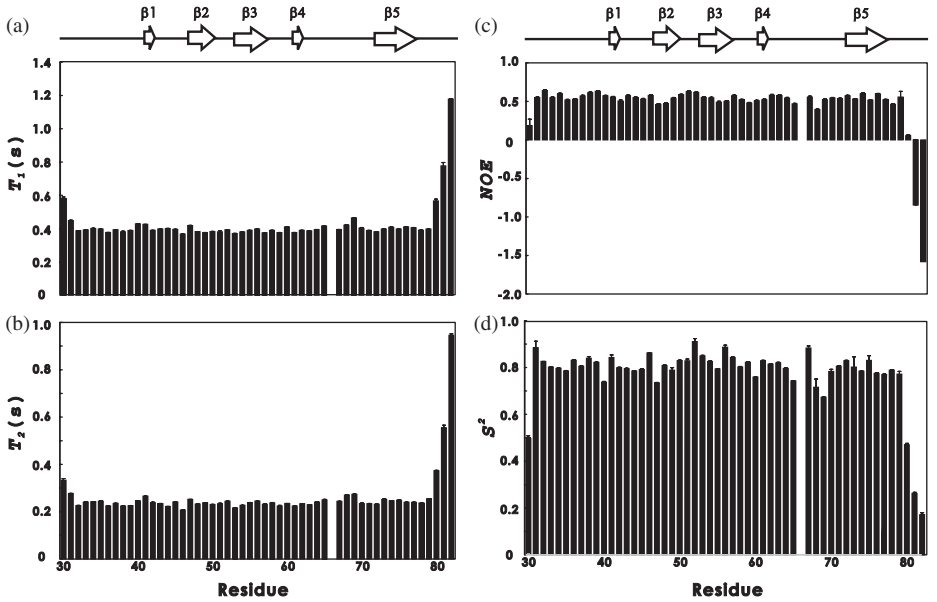

Fig. 4. **Plots of amide ^{15}N T_1, T_2, and NOE against the residue number.** The data were obtained at the ^{15}N resonance frequency of 50.678 MHz, which corresponded to the ^{1}H resonance frequency of 500.13 MHz. (a) Longitudinal relaxation times, T_1, (b) transverse relaxation times, T_2, (c) heteronuclear $\{^{1}H\}$-^{15}N steady-state NOE values defined as $I_{NOE}/I_{NON\text{-}NOE}$, where I_{NOE} and $I_{NON\text{-}NOE}$ are the peak intensities with and without ^{1}H saturation, respectively, and (d) the squared order parameters, S^2, determined on model-free analysis (*32*). The secondary structures are indicated at the top.

maximum of only 0.4 s^{-1}. These results indicated that the overall conformation of $ChBD_{ChiC}$ was stable.

It has often been suggested that a large motion induced by ligand-binding may be predicted by significant R_{ex} terms in the relevant region even in the absence of the ligand. This suggestion is based on the assumption that the conformation of a protein is exchanging in solution between those in its ground and excited states in equilibrium, and that the conformation in one of the exited states should be in accord with that in the ligand-bound form. Recently, this phenomenon was actually observed in a few examples (*37*), and, therefore, this idea has been gradually accepted. In light of the above discussion, the fact that no significant exchange rate, R_{ex}, was observed for $ChBD_{ChiC}$ in its free form may suggest that no large conformational change in its backbone would occur upon binding with chitin. A small conformational change, particularly in the side-chain orientations of the associated tryptophans, might be induced upon interaction, which should be investigated in the future.

DISCUSSION

Comparison of $ChBD_{ChiC}$ *and* $ChBD_{ChiB}$—Structural analysis with the Dali server showed that $ChBD_{ChiB}$ (*36*) had the backbone conformation most similar to that of $ChBD_{ChiC}$ among all the structures that have been already determined and stored in the Protein Data Bank (PDB), with a pairwise RMSD value of Cα atoms of 1.5 Å and a Z-score of 7.3 (Fig. 5). In the discussion below, we have classified $ChBD_{ChiB}$ and $ChBD_{ChiC}$ into the same group considering that both of them share the common feature of possessing two aromatic rings that directly interact with chitin (Trp479 and Tyr481 in $ChBD_{ChiB}$). However, they are slightly different from each other in a few points. First, while $ChBD_{ChiC}$ contains a disulfide bridge between the N- and C-terminal regions, $ChBD_{ChiB}$ does not (Fig. 5). Second, in $ChBD_{ChiB}$, there is a glycine residue (Gly480) between Trp479 and Tyr481. Even with such differences, the local conformations in these regions of $ChBD_{ChiB}$ and $ChBD_{ChiC}$ were very similar; the N- and C-terminal regions of $ChBD_{ChiB}$ are close to each other to such a degree that it was as if there was a disulfide bridge between them. In addition, when their backbones were overlaid, the positions of Trp479 in $ChBD_{ChiB}$ and Trp59 in $ChBD_{ChiC}$, and those of Tyr481 in $ChBD_{ChiB}$ and Trp60 in $ChBD_{ChiC}$ almost completely overlapped.

Comparison of $ChBD_{ChiC}$ *and* CBD_{EGZ}—The backbone conformation of $ChBD_{ChiC}$ that we determined by NMR was very similar to that of CBD_{EGZ} (pairwise RMSD value and Dali Z-score, 1.7 Å and 5.4) (Fig. 5). Furthermore, in $ChBD_{ChiC}$, the aromatic rings of Trp59 and Trp60 were located on the molecular surface and exposed to the solvent in the same way as those of Trp43 and Tyr44 in CBD_{EGZ}, which corresponded respectively to Trp59 and Trp60 in the sequential alignment. Since both these chitin- and cellulose-binding domains belong to CBM family 5, the close resemblance in their conformations is not surprising. However, a remarkable difference was found in the numbers of the aromatic rings that were exposed to the solvent and therefore associated with direct binding to substrates. In CBD_{EGZ}, three aromatic rings, Trp18, Trp43, and Tyr44, were exposed and aligned linearly on one side of the molecular surface, and were supposed to interact directly with the glucose moieties of cellulose (*38*), probably through a hydrophobic interaction and hydrogen-bonds. A set of three aromatic rings with such a character has been observed in a lot of cellulose-binding domains for which the structures have so far been determined, including CBD_{CipB} (*39*), CBD_{Cex} (*40*), and CBD_{CBH1} (*41*, *42*). In $ChBD_{ChiC}$, however, two aromatic rings alone, Trp59 and Trp60, were exposed to the solvent, the remaining one, Trp36, being oriented inwards (Fig. 5a). In fact, alignment based on the structures indicated that Trp36 in $ChBD_{ChiC}$ corresponded to Tyr10 in CBD_{EGZ}, although alignment using their sequences alone incorrectly suggested that Trp18 in CBD_{EGZ} was the residue corresponding to Trp36 in $ChBD_{ChiC}$.

Comparison of $ChBD_{ChiC}$ *and* $ChBD_{ChiA1}$—The position and orientation of Trp36 in $ChBD_{ChiC}$ were also similar to those of Trp656 in $ChBD_{ChiA1}$ (*20*). Although $ChBD_{ChiA1}$ has been classified into CBM family 12, the overall

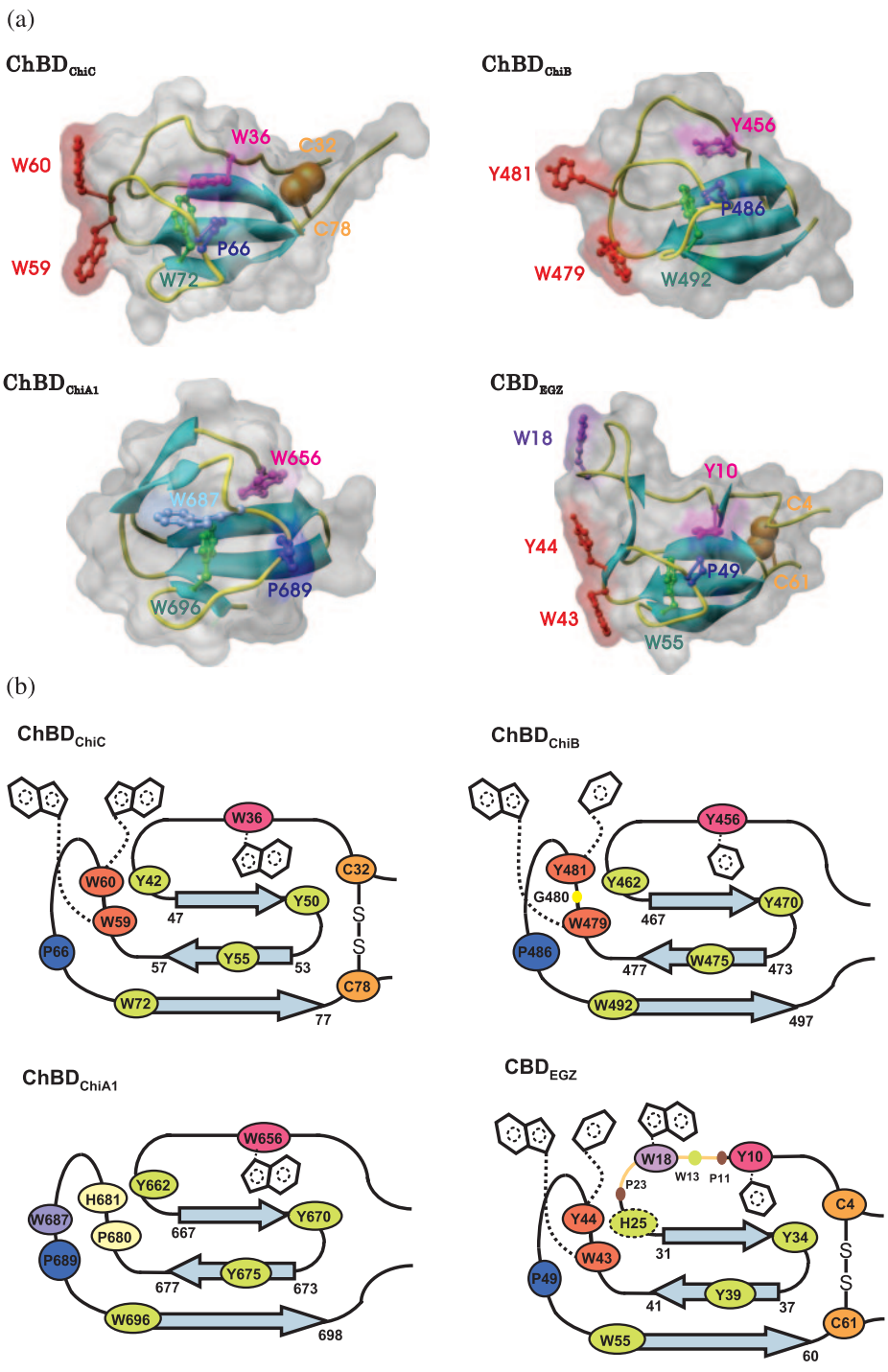

Fig. 5. **Comparison of the three-dimensional structures of representative chitin- and cellulose-binding domains that belong to CBM family 5 or 12.** (a) The solvent accessible surfaces of ChBD$_{ChiC}$, ChBD$_{ChiA1}$, ChBD$_{ChiB}$, and CBD$_{EGZ}$ with a ribbon display for the backbones. Some important residues for structural comparison are displayed as a ball-and-stick model. The sulfur atoms in the disulfide bridges are indicated by yellow balls. The PDB accession codes for these four structures are given in the legend to Fig. 1. The figures were created using Chimera (*35*). (b) Schematic drawing of the structures of ChBD$_{ChiC}$, ChBD$_{ChiA1}$, ChBD$_{ChiB}$, and CBD$_{EGZ}$. The important residues for comparison are indicated.

backbone conformation, especially in the β-sheet regions, of ChBD$_{ChiA1}$ is basically the same as those of CBD$_{EGZ}$ and ChBD$_{ChiC}$ (pairwise RMSD value and Dali Z-score, 1.1 Å and 6.7) (Fig. 5). In addition, some core-forming hydrophobic and aromatic residues that were well conserved among the three binding domains were also similar in their orientations, as seen in Fig. 5. However, these three binding domains have very different interfaces with substrates. CBD$_{EGZ}$ has three aromatic residues that interact with a substrate, and ChBD$_{ChiC}$ has only two such residues, which we have shown directly interact with a substrate. ChBD$_{ChiA1}$ has no such aromatic residue, and no substitute binding interface has been precisely identified, although a distinct region around Trp687 (Fig. 5) has been suggested to be a possible binding surface by mutagenesis experiments (*43*, *44*).

Structural Classification of Binding Domains—The chitin- and cellulose-binding domains that belong to CBM family 5 or 12 can be classified into three or four groups on the basis of their sequences and the structures of CBD$_{EGZ}$, ChBD$_{ChiC}$, ChBD$_{ChiB}$, and ChBD$_{ChiA1}$. The first group, represented by CBD$_{EGZ}$ (colored yellow in Fig. 1),

has three aromatic rings that are aligned linearly, exposed to the solvent, and used for direct interaction with the substrates, as observed for other larger cellulose-binding domains. All the members are likely to contain a relatively flexible loop that is inserted between two prolines (Pro11 and Pro23 in CBD_{EGZ}) with an aromatic ring in the loop (Trp18) exposed to the solvent partly through the *cis* peptide bond of the N-terminal-side proline (Pro11). Some members have a disulfide bridge between the N- and C-terminal regions (Cys4 and Cys61). The second group, represented by $ChBD_{ChiC}$ and $ChBD_{ChiB}$ (colored pink in Fig. 1), has only two aromatic rings that interact directly with substrates because the members lack the flexible loop between the two prolines mentioned above. Most of the members have a disulfide bridge between the N- and C-terminal regions (Cys32 and Cys78 in $ChBD_{ChiC}$). The third group, represented by $ChBD_{ChiA1}$ (colored green in Fig. 1), has no aromatic residue on the surface corresponding to the interaction surfaces in CBD_{EGZ} and $ChBD_{ChiC}$. Although histidine residues (His 681 in $ChBD_{ChiA1}$, as an example) exist in the region, the recently solved crystal structure of $ChBD_{ChiA1}$ and further NMR analysis have shown that the side-chain of the histidine residue faces inwardly, not into the solvent [*Acta Cryst.* (2005) **A61**, C202 for XX Congress of the IUCr2005]. The members have no proline-pinched loop either. Instead of such a set of aromatic rings, they have a characteristic tryptophan residue in the loop between β-strands 4 and 5 (Trp687 in $ChBD_{ChiA1}$, Fig. 5), which is possibly used to interact with substrates. They have no disulfide bridge. The fourth group (colored cyan in Fig. 1) can be separated from these three groups according to their sequential alignments, but is very similar to the $ChBD_{ChiC}$ group. Alternatively, the group can be interpreted as being similar to the CBD_{EGZ} group, assuming that the N-terminal region sandwiched by two prolines, PGEYPAWDP, for example, is of the same kind as those present in the CBD_{EGZ} group (*i.e.*, the loop containing Trp18 in CBD_{EGZ}). Since none of the structures of these members have been determined yet, the classification of this group is ambiguous. All the members of these three or four groups have similar backbone conformations, but have very distinct characters in the most important parts involved in the recognition of the substrates. These differences are interesting in terms of their possibly different interaction mechanisms and of their evolution.

The structures of a lot of cellulose-binding domains (CBDs) have been determined, it being demonstrated that most CBDs, particularly those belonging to CBM family 1, 2, 3, 5, or 10, possess three aromatic residues that are exposed to the solvent and interact with a substrate. For chitin-binding domains (ChBDs), on the other hand, several structures alone are known. Nevertheless, from the high sequence similarities between CBDs and ChBDs within CBM families 2 and 5 (in which both CBDs and ChBDs are included), ChBDs were also supposed to interact with chitin through three characteristic aromatic rings in the same way as CBDs. However, the recently elucidated structures of a few ChBDs including $ChBD_{ChiA1}$, $ChBD_{ChiB}$ (*36*), and $ChBD_{ChiC}$, possessing two or no such aromatic rings, are beginning to throw new light on the number of associated aromatic residues. These rather *irregular* binding surfaces may be limited to ChBDs, belonging to CBM family 5 or 12 in particular, and the different numbers of associated aromatic rings may be a natural consequence of binding to different substrates, *i.e.*, chitin and cellulose. However, our updated sequential alignments for CBM families 5 and 12 based on the structures of CBD_{EGZ} (*18*), $ChBD_{ChiA1}$, $ChBD_{ChiB}$, and $ChBD_{ChiC}$ (Fig. 1) suggest that some CBDs have less than three exposed aromatic rings and that some ChBDs conversely have three, like most CBDs. To clarify this point, we await the structures of other CBDs and ChBDs.

The assigned chemical shifts and the structures of $ChBD_{ChiC}$ have been registered in the BioMagResBank under accession code 10005, and in the Protein Data Bank under accession code 2D49, respectively. We wish to thank Ms. Izumi Yabuta for the helpful discussion. This work was supported in part by the grants for the promotion of Niigata University research projects and for the Protein-3000 project from the Ministry of Education, Culture, Sports, Science, and Technology of Japan.

REFERENCES

1. Kurita, K. (2001) Controlled functionalization of the polysaccharide chitin. *Prog. Polym. Sci.* **26**, 1921–1971
2. Henrissat, B. (1991) A classification of glycosyl hydrolases based on amino acid sequence similarities. *Biochem. J.* **280**, 309–316
3. Henrissat, B. and Bairoch, A. (1993) New families in the classification of glycosyl hydrolases based on amino acid sequence similarities. *Biochem. J.* **293**, 781–788
4. Perrakis, A., Tews, I., Dauter, Z., Oppenheim, A.B., Chet, I., Wilson, K.S., and Vorgias, C.E. (1994) Crystal structure of a bacterial chitinase at 2.3 Å resolution. *Structure* **2**, 1169–1180
5. Davies, G. and Henrissat, B. (1995) Structure and mechanism of glycosyl hydrolases. *Structure* **3**, 853–859
6. Tews, I., Terwissha van Scheltinga, A.C., Perrakis, A., Wilson, K.S., and Dijkatra,B.W. (1997) Substrate-assisted catalysis unifies two families of chitinolytic enzymes. *J. Am. Chem. Soc.* **119**,7954–7959
7. Brameld, K.A., Shrader, W.D., Imperiali, B., and Goddard, W.A. 3rd. (1998) Substrate assistance in the mechanism of family 18 chitinases: theoretical studies of potential intermediates and inhibitors. *J. Mol. Biol.* **280**, 913–923
8. Hart, P.J., Pfluger, H.D., Monzingo, A.F., Hollis, T., and Robertus, J.D. (1995) The refined crystal structure of an endochitinase from *Hordeum vulgare* L. seeds at 1.8 Å resolution. *J. Mol. Biol.* **248**, 402–413
9. Garcia-Casado, G., Collada, C., Allona, I., Casado, R., Pacios, L.F., Aragoncillo, C., and Gomez, L. (1998) Site-directed mutagenesis of active site residues in a class I endochitinase from chestnut seeds. *Glycobiology* **8**, 1021–1028
10. Ohno, T., Armand, S., Hata, T., Nikaidou, N., Henrissat, B., Mitsutomi, M., and Watanabe, T. (1996) A modular family 19 chitinase found in the prokaryotic organism *Streptomyces griseus* HUT 6037. *J. Bacteriol.* **178**, 5065–5070
11. Watanabe, T., Kanai, R., Kawase, T., Tanabe, T., Mitsutomi, M., Sakuda, S., and Miyashita K. (1999) Family 19 chitinases of *Streptomyces* species: characterization and distribution. *Microbiology* **145**, 3353–3363
12. Itoh, Y., Takahashi, K., Takizawa, H., Nikaidou, N., Tanaka, H., Nishihashi, H., Watanabe, T., and Nishizawa, Y. (2003) Family 19 chitinase of *Streptomyces griseus* HUT6037 increases plant resistance to the fungal disease. *Biosci. Biotechnol. Biochem.* **67**, 847–855
13. Tomme, P., Warren, R.A., Miller, R.C., Kilburn, D.G.Jr., and Gilkes, N.R. (1995) Cellulose-binding domains: classification and properties in *Enzymatic Degradation of Insoluble*

Polysaccharides (Saddler, J.N. and Penner, M., eds.) pp. 142–163, American Chemical Society, Washington
14. Collinge, D.B., Kragh, K.M., Mikkelsen, J.D., Nielsen, K.K., Rasmussen, U., and Vad, K. (1993) Plant chitinases. *Plant J.* **3**, 31–40
15. Wright, C.S. (1987) Refinement of the crystal structure of wheat germ agglutinin isolectin 2 at 1.8 Å resolution. *J. Mol. Biol.* **194**, 501–529
16. Hashimoto, M., Ikegami, T., Seino, S., Ohuchi, N., Fukada, H., Sugiyama, J., Shirakawa, M., and Watanabe, T. (2000) Expression and characterization of the chitin-binding domain of chitinase A1 from *Bacillus circulans* WL-12. *J. Bacteriol.* **182**, 3045–3054
17. Jee, J.G., Ikegami, T., Hashimoto, M., Kawabata, T., Ikeguchi, M., Watanabe, T., and Shirakawa, M. (2002) Solution structure of the fibronectin type III domain from *Bacillus circulans* WL-12 chitinase A1. *J. Biol. Chem.* **277**, 1388–1397
18. Brun, E., Moriaud, F., Gans, P., Blackledge, M.J., Barras, F., and Marion, D. (1997) Solution structure of the cellulose-binding domain of the endoglucanase Z secreted by *Erwinia chrysanthemi*. *Biochemistry* **36**, 16074–16086
19. Itoh, Y., Kawase, T., Nikaidou, N., Fukada, H., Mitsutomi, M., Watanabe, T., and Itoh, Y. (2002) Functional analysis of the chitin-binding domain of a family 19 chitinase from *Streptomyces griseus* HUT6037: substrate-binding affinity and *cis*-dominant increase of antifungal function. *Biosci. Biotechnol. Biochem.* **66**, 1084–1092
20. Ikegami, T., Okada, T., Hashimoto, M., Seino, S., Watanabe, T., and Shirakawa, M. (2000) Solution structure of the chitin-binding domain of *Bacillus circulans* WL-12 chitinase A1. *J. Biol. Chem.* **275**, 13654–13661
21. Cavanagh, J., Fairbrother, W.J., Palmer, A.G.III, and Skelton, N.J. (1996) *Protein NMR Spectroscopy*, Academic Press, San Diego
22. Yamazaki, T., Forman-Kay, J.D., and Kay, L.E. (1993) Two-dimensional NMR experiments for correlating $^{13}C\beta$ and $^{1}H\delta/\epsilon$ chemical shifts of aromatic residues in ^{13}C-labeled proteins via scalar couplings. *J. Am. Chem. Soc.* **115**, 11054–11055
23. Delaglio, F., Grzesiek, S., Vuister, G.W., Zhu, G., Pfeifer, J., and Bax, A. (1995) NMRPipe: a multidimensional spectral processing system based on UNIX pipes. *J. Biomol. NMR* **6**, 277–293
24. Goddard, T.D. and Kneller,D.G. *SPARKY 3*, University of California, San Francisco
25. Hu, J.-S., Grzesiek, S., and Bax, A. (1997) Two-dimensional NMR methods for determining χ_1 angles of aromatic residues in proteins from three-bond $J_{C'C\gamma}$ and $J_{NC\gamma}$ couplings. *J. Am. Chem. Soc.* **119**, 1803–1804
26. Wüthrich, K. (1986) *NMR of Proteins and Nucleic Acids*, John Wiley & Sons, New York
27. Güntert, P., Mumenthaler, C., and Wüthrich, K. (1997) Torsion angle dynamics for NMR structure calculation with the new program DYANA. *J. Mol. Biol.* **273**, 283–298
28. Neri, D., Szyperski, T., Otting, G., Senn, H., and Wüthrich, K. (1989) Stereospecific nuclear magnetic resonance assignments of the methyl groups of valine and leucine in the DNA-binding domain of the 434 repressor by biosynthetically directed fractional ^{13}C labeling. *Biochemistry* **28**, 7510–7516
29. Cornilescu, G., Delaglio, F., and Bax, A. (1999) Protein backbone angle restraints from searching a database for chemical shift and sequence homology. *J. Biomol. NMR* **13**, 289–302
30. Laskowski, R.A., Rullmannn, J.A., MacArthur, M.W., Kaptein, R., and Thornton, J.M. (1996) AQUA and PROCHECK-NMR: programs for checking the quality of protein structures solved by NMR. *J. Biomol. NMR* **8**, 477–486
31. Farrow, N.A., Muhandiram, R., Singer, A.U., Pascal, S.M., Kay, C.M., Gish, G., Shoelson, S.E., Pawson, T., Forman-Kay, J.D., and Kay, L.E. (1994) Backbone dynamics of a free and a phosphopeptide-complexed src homology 2 domain studied by ^{15}N NMR relaxation. *Biochemistry* **33**, 5984–6003
32. Lipari, G. and Szabo, A. (1982) Model-free approach to the interpretation of nuclear magnetic resonance relaxation in macromolecules. *J. Am. Chem. Soc.* **104**, 4546–4570
33. Dosset, P., Hus, J.C., Blackledge, M., and Marion, D. (2000) Efficient analysis of macromolecular rotational diffusion from heteronuclear relaxation data. *J. Biomol. NMR* **16**, 23–28
34. Sharma, D. and Rajarathnam, K. (2000) ^{13}C NMR chemical shifts can predict disulfide bond formation. *J. Biomol. NMR* **18**, 165–171
35. Pettersen, E.F., Goddard, T.D., Huang, C.C., Couch, G.S., Greenblatt, D.M., Meng, E.C., and Ferrin, T.E. (2004) UCSF Chimera - A visualization system for exploratory research and analysis. *J. Comput. Chem.* **25**, 1605–1612
36. van Aalten, D.M., Synstad, B., Brurberg, M.B., Hough, E., Riise, B.W., Eijsink, V.G., and Wierenga, R.K. (2000) Structure of a two-domain chitotriosidase from *Serratia marcescens* at 1.9-Å resolution. *Proc. Natl. Acad. Sci. USA* **97**, 5842–5847
37. Eisenmesser, E.Z., Millet, O., Labeikovsky, W., Korzhnev, D.M., Wolf-Watz, M., Bosco, D.A., Skalicky, J.J., Kay, L.E., and Kern, D. (2005) Intrinsic dynamics of an enzyme underlies catalysis. *Nature* **438**, 117–121
38. Simpson, H.D. and Barras, F. (1999) Functional analysis of the carbohydrate-binding domains of *Erwinia chrysanthemi* Cel5 (Endoglucanase Z) and an *Escherichia coli* putative chitinase. *J. Bacteriol.* **181**, 4611–4616
39. Tormo, J., Lamed, R., Chirino, A.J., Morag, E., Bayer, E.A., Shoham, Y., and Steitz, T.A. (1996) Crystal structure of a bacterial family-III cellulose-binding domain: a general mechanism for attachment to cellulose. *EMBO J.* **15**, 5739–5751
40. Xu, G.Y., Ong, E., Gilkes, N.R., Kilburn, D.G., Muhandiram, D.R., Harris-Brandts, M., Carver, J.P., Kay, L.E., and Harvey, T.S. (1995) Solution structure of a cellulose-binding domain from *Cellulomonas fimi* by nuclear magnetic resonance spectroscopy. *Biochemistry* **34**, 6993–7009
41. Kraulis, J., Clore, G.M., Nilges, M., Jones, T.A., Pettersson, G., Knowles, J., and Gronenborn, A.M. (1989) Determination of the three-dimensional solution structure of the C-terminal domain of cellobiohydrolase I from *Trichoderma reesei*. A study using nuclear magnetic resonance and hybrid distance geometry-dynamical simulated annealing. *Biochemistry* **28**, 7241–7257
42. Mattinen, M.L., Kontteli, M., Kerovuo, J., Linder, M., Annila, A., Lindeberg, G., Reinikainen, T., and Drakenberg, T. (1997) Three-dimensional structures of three engineered cellulose-binding domains of cellobiohydrolase I from *Trichoderma reesei*. *Protein Sci.* **6**, 294–303
43. Ferrandon, S., Sterzenbach, T., Mersha, F.B., and Xu, M.Q. (2003) A single surface tryptophan in the chitin-binding domain from *Bacillus circulans* chitinase A1 plays a pivotal role in binding chitin and can be modified to create an elutable affinity tag. *Biochim. Biophys. Acta* **1621**, 31–40
44. Hardt, M. and Laine, R.A. (2004) Mutation of active site residues in the chitin-binding domain $ChBD_{ChiA1}$ from chitinase A1 of *Bacillus circulans* alters substrate specificity: use of a green fluorescent protein binding assay. *Arch. Biochem. Biophys.* **426**, 286–297
45. Thompson, J.D., Higgins, D.G., and Gibson, T.J. (1994) CLUSTAL W: improving the sensitivity of progressive multiple sequence alignment through sequence weighting, position-specific gap penalties and weight matrix choice. *Nucleic Acids Res.* **22**, 4673–4680
46. Holm, L. and Sander, C. (1993) Protein structure comparison by alignment of distance matrices. *J. Mol. Biol.* **233**, 123–138
47. Koradi, R., Billeter, M., and Wüthrich, K. (1996) MOLMOL: a program for display and analysis of macromolecular structures. *J. Mol. Graph.* **14**, 51–55